Body Shape and Orientation Control for Locomotion of Biologically-Inspired Snake Robots

Ehsan Rezapour, Kristin Y. Pettersen, Jan T. Gravdahl, and Pål Liljebäck

Abstract— **This paper considers guidance-based motion control of planar snake robots using a dynamic feedback control law. We first present the Euler-Lagrange equations of motion of the robot. Subsequently, we introduce a dynamic feedback control law for the joints of the robot to track a desired gait pattern. This tracking control law depends on the time evolution of the state variables of a dynamic compensator which is used for controlling the orientation of the robot. In particular, we employ the dynamic compensator to practically stabilize a reference head angle defined by a Line-of-Sight path following guidance law. Using an input-output stability analysis, we show the uniform boundedness of the solutions of the controlled system. Furthermore, we use a perturbation analysis to show that the orientation error is ultimately bounded by an arbitrarily small bound. Simulation results are presented to validate the theoretical results.**

I. INTRODUCTION

Snake robots are a class of biologically inspired robots which emulate the features of biological snakes. Due to their slender structure and many degrees-of-freedom, which makes them capable of moving in narrow and unstructured environments, there is an increasing number of emerging applications of these robots in medical (e.g. image-guided surgery [1], open heart surgery [2]), industrial [3], and search and rescue operations [4]. In addition to their many practical applications, snake robots pose many motion control challenges. These challenges mainly arise due to the complex motion patterns and underactuation issues. Furthermore, the complex dynamical behaviour of these robots gives rise to complicated dynamic models and this makes model-based analysis and control design challenging.

In general, snake robots can be categorized into two classes; snake robots which are equipped with passive wheels, and wheel-less snake robots. Snake robots with passive wheels are subject to nonholonomic velocity constraints, while wheel-less snake robots are unconstrained, i.e. without velocity constraints. Motion control of both classes of snake robots has been considered in several previous works. The majority of these works consider snake robots with passive wheels, which is inspired by the world's first snake robot

developed in 1972 [5], and which introduce sideslip constraints on the links of the robot. These constraints allow the control input to be specified directly in terms of the desired propulsion of the snake robot, which is employed in e.g. [6-9] for computed torque control of the position and orientation of wheeled snake robots. Motion control of fish and eel-like robots is related to the topic of snake robots and is considered in e.g. [6] using motion planning and gait generation methods.

Locomotion control of wheel-less snake robots is only considered in a few previous works. Wheel-less snake robots are interesting for traversing even more challenging environments where the passive wheels may slip or get tangled up in irregularities in the terrain. Methods based on numerical optimal control are considered in [11] for determining optimal gaits during positional control of wheel-less snake robots. In [12-13], cascaded systems theory is employed to achieve path following control of a wheel-less snake robot described by a simplified model. In [14], a virtual holonomic constraints approach is used to control the orientation of the robot to a path following guidance law.

This paper considers both body shape and orientation control of wheel-less planar snake robots. In particular, based on the Euler-Lagrange equations describing the dynamics and kinematics of the snake robot, we design a guidance-based control strategy using a dynamic feedback control law. Guidance-based control strategies are in general based on defining a reference heading angle for the vehicle through a guidance law, and subsequently designing a tracking controller to track this angle [15]. The motivation for this guidance-based control strategy is to solve the path following problem for the snake robot. To our best knowledge, the only previous works which consider guidance-based path following control of wheel-less planar snake robots are [13,14]. In [13], the control design is based on a simplified model of the snake robot which is valid for small joint angles. In the present work we carry out a model-based control design for a wheel-less snake robot based on a more accurate model of the robot which does not consider such simplifying assumptions. In [14], the authors used an approach based on the method of virtual holonomic constraints to control the orientation of the robot. However, the major drawback of [14] was the absence of an analytical proof for the boundedness of the solutions of the dynamic compensator which was used to control the orientation of the robot. In contrast with [14], in this work we employ design and analysis tools from reduction theory and finite-gain $\mathcal{L}$ stability which enable us to analytically show that the body shape variables

achieve perfect tracking, the orientation error converges to an arbitrarily small neighbourhood of the origin, and the states of the dynamic compensator remain bounded.

The paper is organized as follows. In Section II, we present kinematics and dynamics of the snake robot in a Lagrangian framework. In Section III, we state the control design objectives. In Section IV, we consider the design of a tracking controller of the body shape of the robot. In Section V, we develop a guidance-based path following controller for the underactuated position variables of the robot. Finally, in Section VI, the results of the simulations for a snake robot are presented which validate the theoretical results.

II. MODELLING

The kinematic and dynamic models for snake robots are previously derived in several works (e.g. [12,14]). However, for the sake of completeness, we briefly present the highlights of the modelling techniques used in [14] here. For a more comprehensive presentation, please see [14].

For simplicity, we denote the local i-th link frame by $\mathcal{B}_i$, and the inertial frame by $\mathfrak{I}$, cf. Fig 1. We assume that the robot has (N) links with equal length $(2l)$, uniformly distributed mass (m), and moment of inertia (J). To derive the model, we choose the elements of the vector of the configuration variables of the snake robot as

$$x = [q_1, q_2, \ldots, q_{N-1}, \theta_N, p_x, p_y]^T \in \mathbb{R}^{N+2} \quad (1)$$

where $q_a = [q_1, q_2, \ldots, q_{N-1}] \in \mathbb{R}^{N-1}$ is the vector of *shape variables* that define the internal configuration of the robot, and $q_u = [\theta_N, p_x, p_y] \in \mathbb{R}^3$ is the vector of *position variables* that define the head angle and position of the robot in the plane. The overall orientation of the robot is defined as the average of the absolute link angles

$$\bar{\theta} = \frac{1}{N} \sum_{i=1}^{N} \theta_i \quad (2)$$

The planar position of the center of mass (CM) of the robot is defined as $(p_x, p_y) = (\frac{1}{N} \sum_{i=1}^{N} p_{x,i}, \frac{1}{N} \sum_{i=1}^{N} p_{y,i})$. The vector of the generalized velocities is defined as

$$\dot{x} = [\dot{q}_1, \dot{q}_2, \ldots, \dot{q}_{N-1}, \dot{\theta}_N, \dot{p}_x, \dot{p}_y]^T \in \mathbb{R}^{N+2} \quad (3)$$

In order to derive the equations of motion of the snake robot, the kinetic energy of the i-th link is defined as the sum of the translational and rotational kinetic energy as

$$\mathcal{K}_i = \frac{1}{2} m(\dot{p}_{x,i}^2 + \dot{p}_{y,i}^2) + \frac{1}{2} J \dot{\theta}_i^2 \quad (4)$$

The free Lagrangian function $L : \mathbb{R}^{2N+4} \to \mathbb{R}$ of a planar snake robot is equal to the total kinetic energy of the robot:

$$L(x, \dot{x}) = \sum_{i=1}^{N} \mathcal{K}_i(x, \dot{x}) \quad (5)$$

Using the Lagrangian function (5), the controlled Euler-Lagrange equations of motion can be given as

$$\frac{d}{dt} \left(\frac{\partial L}{\partial \dot{x}_i} \right) - \frac{\partial L}{\partial x_i} = (B(x)\tau - \tau_{\text{ext}})_i \quad (6)$$
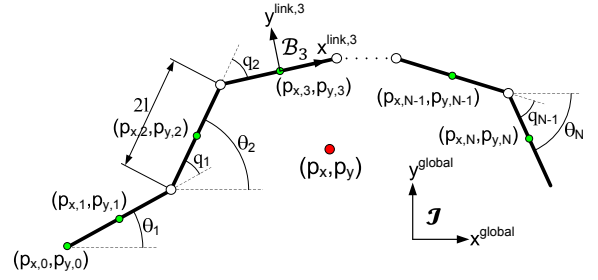

Fig. 1: Kinematic parameters of the snake robot

where $B(x) = [e_j] \in \mathbb{R}^{(N+2) \times (N-1)}$ is the full column rank actuator configuration matrix, with $e_j \in \mathbb{R}^{N+2}$ denoting the j-th standard basis vector in $\mathbb{R}$. Moreover, τ_{ext} denotes the friction forces acting on the system. We can write (6) in the standard second-order form as

$$M(x)\ddot{x} + C(x, \dot{x})\dot{x} = B(x)\tau - \tau_{\text{ext}} \quad (7)$$

where $M(x) \in \mathbb{R}^{(N+2) \times (N+2)}$ is the positive definite symmetric inertia matrix, and $C(x, \dot{x})\dot{x} \in \mathbb{R}^{N+2}$ denotes the generalized Coriolis and centripetal forces. For integrating the effects of friction forces into (7), we first define the rotation matrix for mapping from $\mathfrak{I}$ to $\mathcal{B}_i$ as

$$R_i = \begin{bmatrix} \cos \theta_i & -\sin \theta_i \\ \sin \theta_i & \cos \theta_i \end{bmatrix} \quad (8)$$

Thus, the velocity of the i-th link in $\mathcal{B}_i$ can be written in terms of the velocity of the i-th link in $\mathfrak{I}$ as

$$v_i^{\text{link}} = \begin{bmatrix} v_t^{\text{link},i} & v_n^{\text{link},i} \end{bmatrix}^T = R_i^T \begin{bmatrix} \dot{p}_{x,i} & \dot{p}_{y,i} \end{bmatrix}^T \quad (9)$$

where $v_n^{\text{link},i}$ and $v_t^{\text{link},i}$ denote the linear velocity of the i-th link in the normal and tangential direction of the link, respectively. Assuming equal friction coefficients for all the links, the viscous friction force acting on link i w.r.t. $\mathfrak{I}$ is defined as

$$f_{\text{link},i}^{\text{global}} = R_i [c_t v_t^{\text{link},i}, c_n v_n^{\text{link},i}]^T \in \mathbb{R}^2 \quad (10)$$

where $i \in \{1, \ldots, N\}$, and c_t and c_n denote the viscous friction coefficients in the tangential and normal direction of the link, respectively. We can write τ_{ext} in (7) as

$$\tau_{\text{ext}} = \sum_{i=1}^{N} \mathcal{J}_i^T(x) f_{\text{link},i}^{\text{global}} \quad (11)$$

where

$$\mathcal{J}_i^T(x) = \left[\frac{\partial \dot{p}_{x,i}}{\partial \dot{x}_j}, \frac{\partial \dot{p}_{y,i}}{\partial \dot{x}_j} \right] \in \mathbb{R}^{(N+2) \times 2}, j \in \{1, ..., N+2\}$$

denotes the transpose of the Jacobian matrix of the CM of the i-th link.

To simplify the model-based control design, we write (7) in the partially feedback linearized form. To this end, we follow the approach given in [12], by dividing (1) into two parts as $x = [q_a, q_u]^T \in \mathbb{R}$, and writing (7) as

$$m_{11}(x)\ddot{q}_a + m_{12}(x)\ddot{q}_u + h_1(x, \dot{x}) = \psi \in \mathbb{R}^{N-1} \quad (12)$$

$$m_{21}(x)\ddot{q}_a + m_{22}(x)\ddot{q}_u + h_2(x, \dot{x}) = 0_{3 \times 1} \in \mathbb{R}^3 \quad (13)$$

where $m_{11} \in \mathbb{R}^{(N-1) \times (N-1)}$, $m_{12} \in \mathbb{R}^{(N-1) \times 3}$, $m_{21} \in \mathbb{R}^{3 \times (N-1)}$, and $m_{22} \in \mathbb{R}^{3 \times 3}$ denote the corresponding sub-matrices of the inertia matrix. Moreover, $h_1 \in \mathbb{R}^{N-1}$ and $h_2 \in \mathbb{R}^3$ denote all the contributions of the Coriolis, centripetal and friction forces in (7), and $\psi \in \mathbb{R}^{N-1}$ denotes the non-zero part of the vector of control forces, i.e. $B(x)\tau = [\psi, 0_{3 \times 1}]^T \in \mathbb{R}^{N+2}$. As given in [17], there exists an invertible change of control inputs in the following form, which partially linearizes the dynamic equations (12-13)

$$\psi = \alpha(x)\vartheta + \zeta(x, \dot{x}) \tag{14}$$

where $\vartheta = [\vartheta_1, \ldots, \vartheta_{N-1}]^T \in \mathbb{R}^{N-1}$ denotes the new control inputs, $\alpha(x) = (m_{11} - m_{12} m_{22}^{-1} m_{21})$, and $\zeta(x, \dot{x}) = -(m_{12} m_{22}^{-1}) h_2 + h_1$. Inserting (14) into (12), transforms (12-13) into the following partially feedback linearized form:

$$\ddot{q}_a = \vartheta \in \mathbb{R}^{N-1} \tag{15}$$

$$\ddot{\theta}_N = f_{\theta_N}(x, \dot{x}) + \sum_{i=1}^{N-1} \beta_i(q_a)\vartheta_i \in \mathbb{R} \tag{16}$$

$$\ddot{p}_x = f_x(x, \dot{x}) \in \mathbb{R} \tag{17}$$

$$\ddot{p}_y = f_y(x, \dot{x}) \in \mathbb{R} \tag{18}$$

where $\beta_i : \mathbb{R}^{N-1} \to \mathbb{R}$ is a smooth function. Furthermore, $f = [f_{\theta_N}, f_x, f_y]^T \in \mathbb{R}^3$ represents a vector of Coriolis, centripetal and friction forces.

Assumption I. *We assume that $\sum_{i=1}^{N-1} \beta_i$ is a negative constant.*

Remark I. *Both through numerical simulations and experiments, it can be verified that $\beta_i(q_a)$ is negative-valued for all $i \in \{1, ..., N-1\}$ in any configuration of the robot. This follows from the uniform positive-definiteness of the inertia matrix of the robot. Moreover, $\sum_{i=1}^{N-1} \beta_i$ shows oscillations with a very small magnitude about a negative constant. This negative constant depends on the inertial parameters of the robot, and is always smaller than -1, for any number of links.*

Assumption II. *Throughout this paper we assume that $\sup_{t \geq 0} \|f(x(t), \dot{x}(t))\| < \infty$.*

Assumption II is a realistic assumption, since snake robots often move very slowly, and the external forces due to friction acting on the system will be bounded.

III. CONTROL DESIGN OBJECTIVES

In this work we have two control design objectives. The first objective is to control the internal configuration of the robot, i.e. the body shape of the snake, to provide a desired gait pattern. The second objective is to control the orientation of the robot, which is an underactuated degree of freedom. To achieve these objectives, we first want to stabilize a lateral undulatory gait pattern for the shape variables of the robot. In particular, we define a tracking error variable for the i-th joint of the robot as

$$\tilde{q}_i = q_{\text{ref},i} - q_i \tag{19}$$

where $q_{\text{ref},i}$ denotes the reference i-th joint trajectory which provides the desired gait pattern. (The desired gait pattern will be defined in Section IV). We denote the vector of the

joint tracking errors as $\tilde{q}_a = [\tilde{q}_1, \ldots, \tilde{q}_{N-1}]^T \in \mathbb{R}^{N-1}$. The control objective for the joint angles of the robot can then be defined as asymptotic trajectory tracking such that

$$\lim_{t \to +\infty} \|\tilde{q}_i(t)\| = 0 \tag{20}$$

for every $i \in \{1, \ldots, N-1\}$.

In order to control the planar orientation of the robot, we then need to control the head angle of the robot. Please note that the head angle θ_N, together with the joint angles that give the orientation of the links, $(\theta_1, \ldots, \theta_{N-1})$, give the orientation of the snake robot through (2). We define the tracking error variable for the head angle of the robot as

$$\tilde{\theta} = \theta_{\text{ref}} - \theta_N \tag{21}$$

where θ_{ref} denotes the reference head angle which will be defined in Section V. Since we only have $N-1$ independent control inputs, which will be used to control $\tilde{q}_a$, stabilizing the passive degree of freedom (21) is challenging. We aim to achieve practical stability (see e.g. [18]) for this degree of freedom. Thus, the second part of the control objective is to practically stabilize θ_{ref} for the head angle of the robot, i.e.,

$$\lim_{t \to +\infty} \sup \|\tilde{\theta}(t)\| \leq \epsilon \tag{22}$$

where $\epsilon \in \mathbb{R}_{>0}$ is any positive constant. We also require that all the states of the controlled system remain bounded.

IV. TRACKING CONTROL FOR THE BODY SHAPE

It is known [5] that the gait pattern lateral undulation, which is the most common form of motion pattern among biological snakes, for a snake robot is achieved if each i-th joint of the robot moves according to the reference joint trajectory given by

$$q_{\text{ref},i} = \alpha \sin(\omega t + (i-1)\delta) + \phi_o \tag{23}$$

where α denotes the amplitude of the sinusoidal joint motion, ω denotes the angular frequency, δ is a phase shift that is used to keep the joints out of phase, and ϕ_o is a joint offset that is identical for all of the joints.

To design a tracking controller for the joints of the snake robot, we define the following control law for the i-th joint of the robot

$$\vartheta_i = \ddot{q}_{\text{ref},i} + k_d \dot{\tilde{q}}_i + k_p \tilde{q} \tag{24}$$

where $\vartheta_i \in \{\vartheta_1, \vartheta_2, \ldots, \vartheta_{N-1}\}$ denotes the input to the i-th joint, and $k_p > 0$ and $k_d > 0$ denote the joint controller gains which are chosen identical for all the links since they have similar inertial parameters. By substituting (24) into (15), the equation of the error dynamics for the i-th joint of the snake robot takes the form

$$\ddot{\tilde{q}}_i + k_d \dot{\tilde{q}}_i + k_p \tilde{q}_i = 0 \tag{25}$$

which clearly has a globally exponentially stable equilibrium at the origin $(\tilde{q}_i, \dot{\tilde{q}}_i) = (0, 0)$. This implies that the joint tracking errors converge exponentially fast to zero, regardless of the initial conditions. Consequently, the control objective (20) will be achieved.

V. ORIENTATION CONTROL

In this section, we develop an orientation controller for the snake robot. To this end, we first define a reference head angle for the robot through a path following guidance law, and subsequently, we design a dynamic compensator which controls the head angle of the robot to the defined reference.

A. The Path Following Guidance Law

In this subsection, we define a Line-of-Sight (LOS) guidance law as the reference head angle for the robot. In general, guidance-based control strategies are a common approach for e.g. marine control systems, (see e.g. [15]). These control strategies are based on defining a reference heading angle for the vehicle through a guidance law, and subsequently designing a controller to track this angle. The motivation for this choice is that the LOS guidance law then makes the distance between the vehicle and the path converge to zero, i.e. it makes the vehicle converge to the path. In [13], it was shown that a similar guidance-based control strategy can successfully steer the snake robot towards a desired planar path, and drive the robot along the path. However, in [13] the control design was based on a simplified model of the snake robot which approximated the rotational motion of the links with translational motions which is valid only for small joint angles. In this work we use a similar LOS guidance law for the snake robot. In contrast with [13], however, the tracking control laws are derived based on the dynamic model of the robot that we derived in Section II, without the simplifying assumptions in [13].

Without loss of generality we assume that the desired path is always aligned with the global x-axis. Consequently, the position p_y of the CM of the robot along the y-axis defines the shortest distance between the robot and the desired path, which is often referred to as the *cross-track* error. We then define the LOS path following guidance law, giving the reference head angle for the robot, as a function of the cross-track error as follows

$$\theta_{\text{ref}} = -\operatorname{atan2}\left(\frac{p_y}{\Delta}\right) \qquad (26)$$

where $\Delta > 0$ is a design parameter that is called the look-ahead-distance. The idea of the LOS guidance law (26) is that steering the head angle of the snake robot such that the robot is headed towards a point which is located at a distance Δ ahead of the robot on the desired path, will make the position of the CM of the robot converge to and follow the desired straight path.

B. Head angle control

In this subsection, we propose a tracking control law for the head angle of the robot to track the reference head angle calculated by the guidance law (26). Moreover, we show that the tracking error is ultimately bounded with a bound that can be made arbitrarily small.

It was illustrated in [12] that the offset value ϕ_o defined in (23) can be used to reorient the snake robot in the plane. Based on this knowledge, the main idea of our control design for the orientation of the robot is to use $\ddot{\phi}_o$ in the form

of a dynamic compensator which reorients the robot in the plane through adding an appropriately defined offset angle to each link of the robot, i.e. in accordance with (26). In particular, we design this term to practically stabilize the reference head angle (26) for the robot, and thereby achieving the control objective (22). Moreover, we show that the states of the dynamic compensator remain uniformly bounded.

With the gait pattern lateral undulation in (23), the reference trajectories for the joints of the snake robot are composed of non-identical sinusoidal parts and an identical offset term. In particular, by taking $S_i = \alpha \sin(\omega t + (i-1)\delta)$, the reference trajectory of the i-th joint can be denoted as

$$q_{\text{ref},i} = S_i + \phi_o \qquad (27)$$

The closed-loop dynamics of the head angle can be obtained by inserting the control law (24) into (16) which gives (arguments are excluded for notational convenience)

$$\ddot{\theta}_N = f_{\theta_N} + \sum_{i=1}^{N-1} \beta_i \vartheta_i =$$
$$f_{\theta_N} + \sum_{i=1}^{N-1} \beta_i (\ddot{S}_i + k_d \dot{S}_i + k_p S_i - k_p q_i - k_d \dot{q}_i) +$$
$$\sum_{i=1}^{N-1} \beta_i (\ddot{\phi}_o + k_p \phi_o + k_d \dot{\phi}_o) \qquad (28)$$

We choose $\ddot{\phi}_o$, utilizing that this can be used as an additional control input, in the form

$$\ddot{\phi}_o = \frac{1}{\sum_{i=1}^{N-1} \beta_i} \left(-f_{\theta_N} - \sum_{i=1}^{N-1} \beta_i (\ddot{S}_i + k_d \dot{S}_i + k_p S_i \right.$$
$$\left. - k_p q_i - k_d \dot{q}_i + 2k_p \phi_o + 2k_d \dot{\phi}_o + \sigma) \qquad (29)$$

where σ is a new control input which will be defined later in this section. Note that β_i is negative-valued for all $i \in \{1, \ldots, N-1\}$, which implies that (29) is globally well-defined. The global exponential stability of the origin of the joint angle error dynamics in (25) implies that the joint tracking errors $(\tilde{q}_i, \dot{\tilde{q}}_i)$ converge exponentially fast to zero. Consequently, the reduced form of (29) to the invariant manifold where $(\tilde{q}_a, \dot{\tilde{q}}_a) = (0_{N-1}, 0_{N-1})$, i.e. where $(q_i, \dot{q}_i) = (S_i + \phi_o, \dot{S}_i + \dot{\phi}_o)$, can be written as

$$\ddot{\phi}_o + k_d \dot{\phi}_o + k_p \phi_o = f_\Phi \qquad (30)$$

where the right-hand side (RHS) function is of the form

$$f_\Phi = \frac{1}{\sum_{i=1}^{N-1} \beta_i} \left(-f_{\theta_N} - \sum_{i=1}^{N-1} \beta_i \ddot{S}_i + \sigma \right) \qquad (31)$$

We denote (30) as the Φ-subsystem. Note that the tracking control law (24) then is a dynamic feedback law, in the sense that it depends on the time evolution of $(\phi_o, \dot{\phi}_o)$, which are the solutions of the dynamical system (30).

In order to control the head angle of the robot, we define the control term σ in (29) as

$$\sigma = \ddot{\theta}_{\text{ref}} + k_{\theta,d} \dot{\tilde{\theta}} + k_{\theta,p} \tilde{\theta} \qquad (32)$$

where $k_{\theta,p} > 0$ and $k_{\theta,d} > 0$ are the head angle controller gains. By inserting (32) into (29), and then the resulting equation into (28), the reduced form of the error dynamics equation for the head angle of the robot to the invariant manifold where $(\tilde{q}_a, \dot{\tilde{q}}_a) = (0_{N-1}, 0_{N-1})$, can be written as

$$\ddot{\tilde{\theta}} + k_{\theta,d}\dot{\tilde{\theta}} + k_{\theta,p}\tilde{\theta} = f_\Theta \qquad (33)$$

We denote (33) as the Θ-subsystem, where the perturbing term on the RHS is of the form

$$f_\Theta(\phi_o, \dot{\phi}_o) = -k_p\phi_o - k_d\dot{\phi}_o \qquad (34)$$

For the aim of analysis, we divide the input to the Φ-subsystem f_Φ given by (31), into two parts. In particular, one part depends on the solutions of the Θ-subsystem, which are the head angle tracking errors, and the other part includes uniformly bounded friction forces and time-dependent reference signals. Consequently, we divide it into

$$f_\Phi = f_{\Phi_1} + f_{\Phi_2} \qquad (35)$$

where

$$f_{\Phi_1} = \frac{1}{\sum_{i=1}^{N-1} \beta_i}(k_{\theta,d}\dot{\tilde{\theta}} + k_{\theta,p}\tilde{\theta})$$

$$f_{\Phi_2} = \frac{1}{\sum_{i=1}^{N-1} \beta_i}\left(-f_{\theta_N} - \sum_{i=1}^{N-1}\beta_i\ddot{S}_i + \ddot{\theta}_{\text{ref}}\right) \qquad (36)$$

Since the input to the Φ-subsystem depends on the solutions of the Θ-subsystem and vice versa, one may verify that the $(\Phi - \Theta)$-subsystems are feedback connected. This interconnection is illustrated in Fig. 2, and can be represented as

$$\Sigma_{int} \begin{cases} \ddot{\tilde{\theta}} &= -k_{\theta,d}\dot{\tilde{\theta}} - k_{\theta,p}\tilde{\theta} + f_\Theta(\phi_o, \dot{\phi}_o) \\ \ddot{\phi}_o &= -k_d\dot{\phi}_o - k_p\phi_o + f_\Phi(t, \tilde{\theta}, \dot{\tilde{\theta}}) \end{cases} \qquad (37)$$

The feedback connected system Σ_{int} is the dynamical system which governs the interconnection between the actuated and underactuated dynamics of the robots in closed-loop. In particular, for the Φ-subsystem, the objective is to keep the solutions bounded, while for the Θ-subsystem, the objective is to drive the solutions to a small neighbourhood of the origin, i.e. to make the head angle error become arbitrarily small. To achieve these objectives, in the following we analyze the conditions under which the feedback connection remains stable.

B.1. Input-Output Stability of the Feedback Connected System

The feedback connected system Σ_{int} is composed of two subsystems given by

$$\frac{d}{dt}\begin{bmatrix} \tilde{\theta} \\ \dot{\tilde{\theta}} \end{bmatrix} = \begin{bmatrix} 0 & 1 \\ -k_{\theta,p} & -k_{\theta,d} \end{bmatrix}\begin{bmatrix} \tilde{\theta} \\ \dot{\tilde{\theta}} \end{bmatrix} + \begin{bmatrix} 0 \\ f_\Theta \end{bmatrix} \qquad (38)$$

$$\frac{d}{dt}\begin{bmatrix} \phi_o \\ \dot{\phi}_o \end{bmatrix} = \begin{bmatrix} 0 & 1 \\ -k_p & -k_d \end{bmatrix}\begin{bmatrix} \phi_o \\ \dot{\phi}_o \end{bmatrix} + \begin{bmatrix} 0 \\ f_\Phi \end{bmatrix} \qquad (39)$$

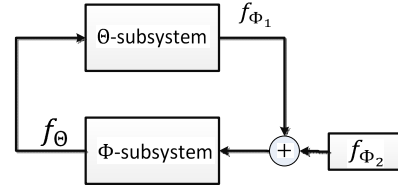To investigate the input-output stability of Σ_{int}, we intro-

Fig. 2: Illustration of the feedback connection (37)

duce the augmented state vector $\hat{x} = [\tilde{\theta}, \phi_o, \dot{\tilde{\theta}}, \dot{\phi}_o]^T \in \mathbb{R}^4$, and the following augmented linear time-invariant system

$$\dot{\hat{x}} = \hat{A}\hat{x} + \hat{B}u \qquad (40)$$
$$y = \hat{C}\hat{x} \qquad (41)$$

where $\hat{A}$ denotes the following matrix

$$\hat{A} = \begin{bmatrix} 0 & 0 & 1 & 0 \\ 0 & 0 & 0 & 1 \\ -k_{\theta,p} & -k_p & -k_{\theta,d} & -k_d \\ \frac{k_{\theta,p}}{\sum_{i=1}^{N-1}\beta_i} & -k_p & \frac{k_{\theta,d}}{\sum_{i=1}^{N-1}\beta_i} & -k_d \end{bmatrix} \qquad (42)$$

and the input u is given by the following uniformly bounded scalar-valued function

$$u = f_{\Phi_2} \qquad (43)$$

The input matrix $\hat{B}$ and the output matrix $\hat{C}$ are, respectively, given by

$$\hat{B} = \begin{bmatrix} 0 & 0 & 0 & 1 \end{bmatrix}^T \qquad (44)$$
$$\hat{C} = \begin{bmatrix} 1 & 1 & 1 & 1 \end{bmatrix} \qquad (45)$$

The following theorem investigates the input-output stability of the augmented dynamical system (40), with the output function (41).

Theorem I. *The augmented dynamical system (40-41), i.e. the feedback connected system Σ_{int}, is finite-gain $\mathcal{L}_2$ stable.*

Proof: It can be verified that all the eigenvalues of matrix $\hat{A}$ have negative real parts, i.e. that matrix $\hat{A}$ is Hurwitz, when $k_p, k_d, k_{\theta,p}, k_{\theta,d} > 0$. Consequently, by [16, Corollary 5.2], we conclude that (40) is finite-gain $\mathcal{L}_p$ stable, for each $p \in [1, \infty]$, and the finite-gain is given by

$$\gamma = \frac{2\lambda_{\max}^2(\hat{P})\|\hat{B}\|_2\|\hat{C}\|_2}{\lambda_{\min}(\hat{P})} \qquad (46)$$

where $\hat{P}$ is the symmetric positive definite matrix solution of the Lyapunov equation

$$\hat{A}^T\hat{P} + \hat{P}\hat{A} = -I \qquad (47)$$

where $I \in \mathbb{R}^{2\times 2}$ denotes the identity matrix. ∎

Remark III. *Based on the finite-gain $\mathcal{L}_2$ stability of Σ_{int}, and uniform boundedness of the exogenous input f_{Φ_2}, we can conclude that the solutions of Σ_{int} are uniformly bounded by*

$$\|y(t)\|_2 \leq \gamma\|u(t)\|_2 \qquad (48)$$

Furthermore, if we denote the upper-bound on the exogenous input f_{Φ_2} as $\zeta_1 = \sup_{t \geq 0}\{f_{\Phi_2}(t)\}$, then we can derive the upper-bound on the solutions $\Phi(t)$ of the dynamic compensator, i.e. the Φ-subsystem, as

$$\zeta = \|\Phi(t)\|_2 \leq \gamma\zeta_1 \in \mathbb{R}_{>0} \tag{49}$$

This upper-bound will be used in the stability analysis presented in the next subsection.

Theorem I guarantees the boundedness of the solutions of the feedback connected system Σ_{int}, and thus the requirement for the boundedness of the states of the dynamic compensator is fulfilled. It remains to show that the head angle error can be made arbitrarily small, which is the subject of the next subsection.

B.2. Practical Stability of the Head Angle Error Dynamics

We denote the state vector of (38) by $\Theta_s = [\tilde{\theta}, \dot{\tilde{\theta}}]^T \in \mathbb{R}^2$, and the state vector of (39) by $\Phi_s = [\phi_o, \dot{\phi}_o]^T \in \mathbb{R}^2$. The dynamical system (38) with $f_\Theta \equiv 0$ denotes the nominal part of the Θ-subsystem, and the dynamical system (39) with $f_\Phi \equiv 0$ denotes the nominal part of the Φ-subsystem. The nominal part of the Θ-subsystem (38), which characterizes the dynamics of the head angle tracking error, has a globally exponentially stable equilibrium at the origin $(\tilde{\theta}, \dot{\tilde{\theta}}) = (0, 0)$ because the following matrix is Hurwitz

$$A = \begin{bmatrix} 0 & 1 \\ -k_{\theta,p} & -k_{\theta,d} \end{bmatrix} \tag{50}$$

However, this nominal part is perturbed by the bounded non-vanishing perturbation term f_Θ. Through the following theorem, we investigate the practical stability of the origin of (38) in the presence of f_Θ.

Theorem II. *Given the feedback connected system (38-39), the head angle error $(\tilde{\theta}, \dot{\tilde{\theta}})$ is uniformly ultimately bounded. Furthermore, it is possible to make the ultimate bound arbitrarily small by choosing sufficiently large gains $(k_{\theta,p}, k_{\theta,d})$.*

Proof: We select a quadratic Lyapunov function in the form

$$V = \frac{1}{2}\Theta_s^T P \Theta_s \tag{51}$$

where $P \in \mathbb{R}^{2 \times 2}$ is the solution of the Lyapunov equation

$$A^T P + PA = -Q \tag{52}$$

Since the matrix A in (50) is Hurwitz, there will always be a unique, symmetric and positive definite solution P to (52) for any positive definite matrix Q [16, Th. 4.6]. In order to reflect that the convergence rate of the linear system given by (50) will depend on the chosen gain parameters, we choose the following $Q \in \mathbb{R}^{2 \times 2}$ positive definite matrix

$$Q = \begin{bmatrix} k_{\theta,p} & 0 \\ 0 & k_{\theta,d} \end{bmatrix} \tag{53}$$

We denote the minimum eigenvalue of Q by $\lambda_{\min}(Q)$, which is characterized by the choice of the head angle controller gains $(k_{\theta,p}, k_{\theta,d})$. By a *Converse Lyapunov Theorem*, expo-

nential stability of the nominal part of (38) implies that (51) satisfies the following inequalities [16, Ch. 9.1]

$$\lambda_{\min}(P)\|\Theta_s\|_2^2 \leq V(\Theta_s) \leq \lambda_{\max}(P)\|\Theta_s\|_2^2$$
$$\frac{\partial V(\Theta_s)}{\partial \Theta_s} A\Theta_s \leq -\lambda_{\min}(Q)\|\Theta_s\|_2^2 \tag{54}$$
$$\left\|\frac{\partial V(\Theta_s)}{\partial \Theta_s}\right\|_2 \leq 2\lambda_{\max}(P)\|\Theta_s\|_2$$

where $\lambda_{\min}(P)$ and $\lambda_{\max}(P)$ denote the minimum and maximum eigenvalues of P, respectively. Furthermore, we select V as a Lyapunov function *candidate* for the perturbed system (38). Taking the time-derivative of V along the solutions of (38), and utilizing the properties (54), gives

$$\dot{V} = -\frac{\partial V}{\partial \Theta_s}A\Theta_s + \frac{\partial V}{\partial \Theta_s}f_\Theta \tag{55}$$

The first RHS term in (55) denotes the time-derivative of V along the solutions of the nominal part of (38), and the second RHS term is the effect of the perturbing term f_Θ. Using the inequalities in (54), we obtain

$$\dot{V} \leq -\lambda_{\min}(Q)\|\Theta_s\|_2^2 + 2\lambda_{\max}(P)\|\Theta_s\|_2\|f_\Theta\|_2 \tag{56}$$

Moreover, from (34) and using Cauchy-Schwartz inequality we have that

$$\|f_\Theta\|_2 \leq \left(\sqrt{k_p^2 + k_d^2}\right)\|\Phi_s\|_2 \tag{57}$$

To simplify the analysis, we choose the controller gains as

$$k_p = \frac{k_p^*}{2\lambda_{\max}(P)}, \quad k_d = \frac{k_d^*}{2\lambda_{\max}(P)} \tag{58}$$

where $k_p^* > 0$ and $k_d^* > 0$. With this choice of controller gains, and also based on the upper-bound on the solutions of the dynamic compensator ζ in (49), inequality (56) takes the form

$$\dot{V} \leq -\lambda_{\min}(Q)\|\Theta_s\|_2^2 + \|\Theta_s\|_2\left(\sqrt{k_p^{*2} + k_d^{*2}}\right)\zeta \tag{59}$$

For the second term in the RHS of (59), we use Young's inequality where we have that

$$ab \leq \frac{\gamma a^2}{2} + \frac{b^2}{2\gamma} \tag{60}$$

where $a, b \in \mathbb{R}$, and $\gamma > 0$ is any positive constant [19]. In particular, by taking

$$a = \|\Theta_s\|_2\left(\sqrt{k_p^{*2} + k_d^{*2}}\right), \quad b = \zeta$$

one can write (59) in the form

$$\dot{V} \leq \left(-\lambda_{\min}(Q) + \gamma\left[k_p^{*2} + k_d^{*2}\right]\right)\|\Theta_s\|_2^2 + \frac{\zeta^2}{2\gamma} \tag{61}$$

With any choice of γ, k_p^*, and k_d^*, we can choose the elements of Q, i.e. $(k_{\theta,p}, k_{\theta,d})$, sufficiently large, so that

$$\alpha^* = \left(-\lambda_{\min}(Q) + \gamma\left[k_p^{*2} + k_d^{*2}\right]\right) \tag{62}$$

is negative. In this case, for a sufficiently small positive

constant λ the following inequality holds

$$\dot{V} \leq -\alpha^* \|\Theta_s\|_2^2 + \frac{\zeta^2}{2\gamma} \leq -\lambda \left(\lambda_{\max}(P)\|\Theta_s\|_2^2\right) + \frac{\zeta^2}{2\gamma} \quad (63)$$

Based on the first inequality in (54), we can also derive the inequality $-\lambda V \geq -\lambda \left(\lambda_{\max}(P)\|\Theta_s\|_2^2\right)$, and using this in (63) yields

$$\dot{V} \leq -\lambda V + \frac{\zeta^2}{2\gamma} \quad (64)$$

Consequently, a straightforward application of the *Comparison Lemma* (see e.g. [16]) yields

$$V(t) \leq e^{-\lambda t} V(0) + \frac{\zeta^2}{2\gamma\lambda} \quad (65)$$

From (65) we conclude the ultimate boundedness of the head angle error, because the first term on the RHS of (65) vanishes as $t \to \infty$, and the second term is uniformly bounded. However, boundedness of the head angle error is not sufficient to achieve the control objective (22). We also need to show that the ultimate bound can be made arbitrarily small. To this end, we notice that based on (65) V converges to a ball of radius $\zeta^2/2\gamma\lambda$. Consequently, based on the inequality $\lambda_{\min}(P)\|\Theta_s\|_2^2 \leq V$ in (54), we conclude that $\|\Theta_s\|_2$ also converges to a ball of radius

$$r = \zeta / \left(\sqrt{2\lambda_{\min}(P)\gamma\lambda}\right) \quad (66)$$

Moreover, we can drive $\|\Theta_s\|_2$ to any arbitrary small neighbourhood of the origin ϵ, by choosing

$$\gamma = \zeta / \left(2\lambda_{\min}(P)\lambda\epsilon^2\right) \quad (67)$$

which can be seen by inserting (67) into (66). Furthermore, from (62) it can be seen that for any value of γ in (67), it is always possible to make α^* negative by making $\lambda_{\min}(Q)$ large enough, i.e. by choosing $(k_{\theta,p}, k_{\theta,d})$ sufficiently large. Consequently, an arbitrarily small ultimate bound for the head angle error can be achieved by properly choosing the gains $(k_{\theta,p}, k_{\theta,d})$, and the control objective (22) is achieved. Moreover, this completes the proof of theorem. ∎

Remark IV. *By the result of Theorem I, the feedback connection (38-39) is finite-gain $\mathcal{L}_2$ stable when $k_p, k_d, k_{\theta,p}, k_{\theta,d} > 0$. Furthermore, from (58) we see that we need to choose the gains of the orientation controller $(k_{\theta,p}, k_{\theta,d})$ sufficiently larger than the gains of the dynamic compensator (k_p, k_d), in order to guarantee that the head angle error converges to a small neighbourhood of the origin. This can also be interpreted based on the fact that (k_p, k_d) increase the strength of the perturbing term f_Θ on the RHS of (38). In other words, by decreasing the strength of f_Θ and increasing $(k_{\theta,p}, k_{\theta,d})$, any small ultimate bound on the head angle error can be achieved.*

VI. SIMULATION RESULTS

In this section we present the results of numerical simulations which illustrate the performance of the proposed control design. We considered a snake robot with $N = 4$ links and with inertial link parameters $m = 0.3$ kg, $l = 0.1$ m, and $J = 0.0016$ kgm^2. The friction coefficients were $c_n = 10$, and $c_t = 1$. The parameters of the reference joint trajectories were $\alpha = 30\pi/180$ rad, $\omega = \pi$ rad/s, and $\delta = 120\pi/180$ rad. The dynamic feedback controller gains were tuned as $k_p = 5$, $k_d = 5$, $k_{\theta,p} = 500$, and $k_{\theta,d} = 500$. Note that we have chosen the gains in accordance with Remarks IV, such that the system is finite-gain $\mathcal{L}_2$ stable, and the orientation error goes to a small neighbourhood of the origin. The lookahead-distance was $\Delta = 3$ m.

As seen from the simulation results, the snake robot successfully tracks the reference body shape and orientation, and thereby converges to and follows the desired path. In particular, Fig. 3 shows that the states of the dynamic compensator remain bounded. Fig. 4 shows that perfect tracking is achieved for the body shape of the robot, and Fig. 5 shows the time evolution of the link angles. Moreover, in Fig. 5 the head angle tracks the LOS guidance law, while the tracking error converges to a neighbourhood of zero as shown in Fig. 6. Finally, Fig. 7 shows how the snake robot successfully converges to and follows the desired path.

VII. CONCLUSION

In this paper we considered the problem of guidance-based path following control of wheel-less planar snake robots using a dynamic feedback controller. The Euler-Lagrange equations of motion were presented. A dynamic tracking control law was proposed for the joints of the snake robot to track a desired gait pattern. In particular, we introduced an extra dynamic variable to the reference joint trajectories, and we used this variable as an additional control for the underactuated degrees of freedom of the robot. Furthermore, through this control term we stabilized a reference head angle for the robot which was defined by a path following guidance law. We showed that the head angle tracking error was ultimately bounded with an arbitrarily small bound. Simulation results were presented which validated the theoretical results. The simulations furthermore showed that the proposed dynamic feedback control law made the snake robot converge to the desired path. A formal proof of the convergence to the path remains a topic of future work.
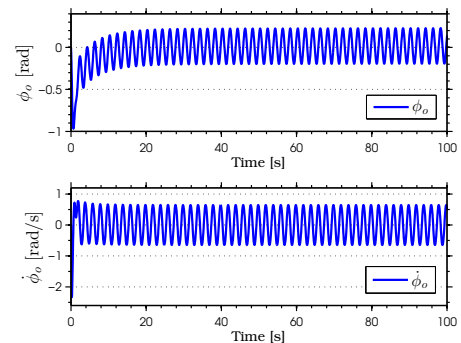

Fig. 3: The solutions of the Φ-subsystem converge to a neighbourhood of the origin after compensating for the head angle error.
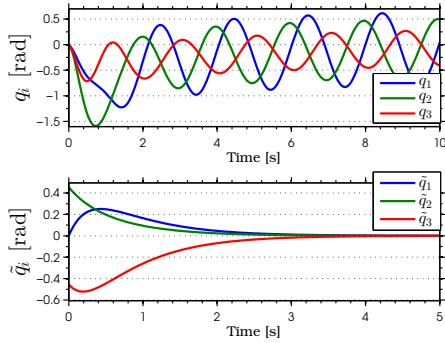
Fig. 4: The joints track the sinusoidal motions (above), the tracking error converges exponentially to zero (below).
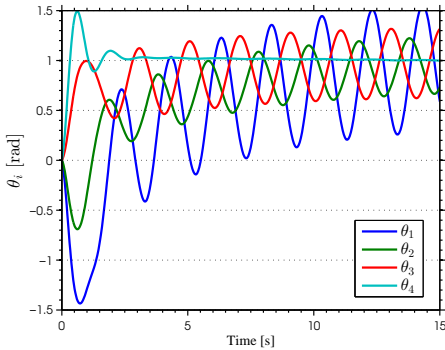

Fig. 5: Oscillations in the links of the robot which are induced by sinusoidal joint motions. The head angle (cyan) tracks the guidance law, and thus does not oscillate.
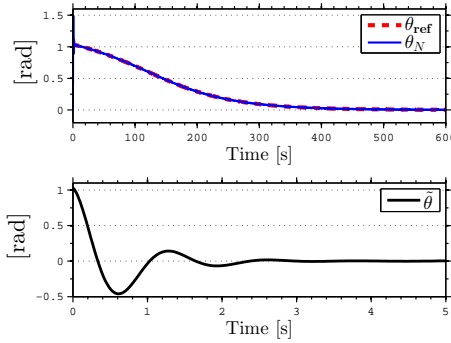

Fig. 6: The head angle tracks the reference head angle (above), the tracking error converges to a neighbourhood of the origin (below).
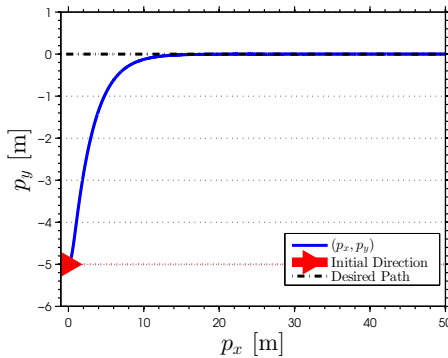

Fig. 7: The robot is initially headed away from the desired path. The position of the CM of the robot (blue) converges to and follows the desired straight line path (the x-axis).

REFERENCES

[1] S. Tully, G. Kantor, M. A. Zenati, and H. Choset, "Shape Estimation for Image-Guided Surgery with a Highly Articulated Snake Robot", Proc. 2011 IEEE/RSJ Int. Conf. on Intelligent Robots and Systems, San Francisco, CA, USA, 2011.

[2] C. Riviere, N. Patronik , and M. Zenati, "Prototype epicardial crawling device for intrapericardial intervention on the beating heart", *Heart Surgery Forum*, Vol. 7, no. 6, pp. 639-643, 2004.

[3] P. Chatzakos, Y. P. Markopoulos, K. Hrissagis, and A. Khalid, "On the development of a modular external-pipe crawling omni-directional mobile robot", *Industrial Robot: An International Journal*, Vol. 33, no. 4, pp. 291-297, 2006.

[4] Z. Wang, and E. Appleton, "The concept and research of a pipe crawling rescue robot.", *Advanced Robotics*, Vol. 17, no. 4, pp: 339-358, 2003.

[5] S. Hirose, "Biologically Inspired Robots: Snake-Like Locomotors and Manipulators", Oxford University Press, 1993.

[6] P. Prautsch, T. Mita, and T. Iwasaki. "Analysis and control of a gait of snake robot", Transactions-Institute of Electrical Engineers of Japan, D-120.3. pp. 372-381. 2000.

[7] H. Date, Y. Hoshi, and M. Sampei, "Locomotion control of a snakelike robot based on dynamic manipulability", in Proc. the IEEE/RSJ Int. Conf. on Intelligent Robots and Systems, Takamatsu, Japan, 2000.

[8] S. Ma, Y. Ohmameuda, K. Inoue, and B. Li, "Control of a 3-dimensional snake-like robot", in Proc. IEEE Int. Conf. Robotics and Automation, vol. 2, Taipei, Taiwan, pp. 2067-2072, 2003.

[9] M. Tanaka and F. Matsuno, "Control of 3-dimensional snake robots by using redundancy", in Proc. IEEE Int. Conf. Robotics and Automation, pp. 1156-1161, Pasadena, CA, 2008. 111-126.

[10] K. McIsaac and J. Ostrowski, "Motion planning for anguilliform locomotion", *IEEE Transactions on Robotics and Automation*, vol. 19, no.4, pp. 637-652, 2003.

[11] G. Hicks and K. Ito, "A method for determination of optimal gaits with application to a snake-like serial-link structure", *IEEE Transactions on Automatic Control*, vol. 50, no. 9, pp. 1291-1306, 2005.

[12] P. Liljebäck, K. Y. Pettersen, Ø. Stavdahl, and J. T. Gravdahl, "Snake Robots - Modelling, Mechatronics, and Control", Advances in Industrial Control, Springer, 2013.

[13] P. Liljebäck, I. U. Haugstuen, and K. Y. Pettersen, "Path following control of planar snake robots using a cascaded approach", *IEEE Transactions on Control Systems Technology*, vol. 20, 111-126, 2012.

[14] E. Rezapour, K.Y. Pettersen, P. Liljebäck, and J.T. Gravdahl, "Path Following Control of Planar Snake Robots Using Virtual Holonomic Constraints", in Proc. IEEE Int. Conf. on Robotics and Biomimetics, Shenzhen, China, 12-14 Dec. 2013.

[15] T. I. Fossen, "Marine control systems: Guidance, navigation and control of ships, rigs and underwater vehicles", Trondheim, Norway: Marine Cybernetics, 2002.

[16] H. K. Khalil, "Nonlinear Systems", Third ed., Englewood cliffs, NJ: Prentice-Hall, 2002.

[17] M. W. Spong, "Underactuated mechanical systems", in Control Problems in Robotics and Automation, B. Siciliano and K. P. Valavanis, Ed., Springer-Verlag, London, UK, 1997.

[18] X. Yang, "Practical stability in dynamical systems", *Chaos, Solitons Fractals*, vol.11 no.7, pp-1087-1092, 2000.

[19] V. I. Arnol'd, "Mathematical methods of classical mechanics", Vol. 60. Springer, 1989.